atmosphere

MDPI

Article

Investigation into the Best Available Moisture Pretreatment Approach for the Measurement of Trichloroethylene and Nitrous Oxide Emitted from Semiconductor Industries

Da-Hyun Baek [1,†], Byeong-Gyu Park [1,†], Sang-Woo Lee [1], Trieu-Vuong Dinh [2,*] and Jo-Chun Kim [1,*]

[1] Department of Civil and Environmental Engineering, Konkuk University, Seoul 05029, Republic of Korea
[2] International Climate and Environmental Research Center, Konkuk University, Seoul 05029, Republic of Korea
* Correspondence: trieuvuong88@konkuk.ac.kr (T.-V.D.); jckim@konkuk.ac.kr (J.-C.K.); Tel.: +82-2-455-0260 (T.-V.D.); Tel.: +82-2-450-4009 (J.-C.K.)
† These authors contributed equally to this work.

Abstract: In this study, the effects of various moisture pretreatment devices (MPDs) on the analytical process of trichloroethylene (TCE) and nitrous oxide (N_2O), which are representative organic and inorganic compounds emitted from semiconductor industries, were investigated. Three types of MPDs—a KPASS (MPD_K), a Nafion™ dryer (MPD_N), and a cooler (MPD_C)—were evaluated for their performance under sample gas conditions of 25 °C and 150 °C at various flow rates. MPD modification was also carried out to improve their performance at high loading capacities. The results indicated that humidity introduced significant bias in the measurement of TCE and N_2O according to the analyzers explored in this study. At a flow rate of 1 L/min, among the MPDs, MPD_N exhibited the highest moisture removal efficiency, followed by MPD_K and MPD_C. In terms of analyte recovery rates, MPD_K achieved the highest TCE recovery, followed by MPD_N and MPD_C, across all tested conditions. Conversely, MPD_C resulted in the lowest N_2O recovery rates, whereas MPD_K and MPD_N maintained over 95% recovery rates. At a flow rate of 4 L/min, MPD_N and MPD_C did not work at high temperatures. In contrast, the modified MPD_K, which received less investment compared to many other membranes, showed an acceptable moisture removal efficiency (>85%) and analyte recovery (>98%). Therefore, modified KPASS is recommended as a useful moisture pretreatment device for the analytical process of TCE and N_2O at both normal and high loading capacities.

Keywords: cooler; KPASS; Nafion dryer; nitrous oxide; trichloroethylene

check for updates

Academic Editor: Evangelos Tolis

Received: 18 February 2025
Revised: 8 April 2025
Accepted: 15 April 2025
Published: 17 April 2025

Citation: Baek, D.-H.; Park, B.-G.; Lee, S.-W.; Dinh, T.-V.; Kim, J.-C. Investigation into the Best Available Moisture Pretreatment Approach for the Measurement of Trichloroethylene and Nitrous Oxide Emitted from Semiconductor Industries. *Atmosphere* **2025**, *16*, 468. https://doi.org/10.3390/atmos16040468

Copyright: © 2025 by the authors. Licensee MDPI, Basel, Switzerland. This article is an open access article distributed under the terms and conditions of the Creative Commons Attribution (CC BY) license (https://creativecommons.org/licenses/by/4.0/).

1. Introduction

Air emission monitoring refers to the systematic collection and analysis of data on air pollutants to evaluate air quality, identify emission sources, and ensure compliance with environmental regulations [1]. This process involves the use of specialized instruments and analytical techniques to quantify pollutant concentrations in ambient air or emissions from stationary sources [1]. Air quality monitoring plays several important roles [1,2]: it enables the detection of hazardous pollutant levels in real time, allowing authorities to issue timely warnings and implement preventive measures; it provides publicly accessible data to enhance public awareness and promote community engagement in air quality improvement; and it supports scientific research on pollution trends, associated health impacts, and the effectiveness of mitigation strategies.

Since the rise in the artificial intelligence era has triggered a race to develop advanced chips, the semiconductor industry has been rapidly expanding in both quantity and quality.

As a result, the emission levels of air pollutants resulting from semiconductor manufacturing have increased. The primary air pollutants such as volatile organic compounds (VOCs), greenhouse gases, inorganic gases, etc., released from semiconductor production are shown in Table 1. Therefore, the emission monitoring for these compounds is necessary.

Table 1. The emission rates and environmental impacts of air pollutants from semiconductor industries in South Korea [3–7].

No.	Compound	Emission (ton/year)	Lifetime	Environmental Effect
1	TVOC	>6000	Few hours to months	Ozone precursor, secondary organic aerosol precursor
2	Trichloroethylene (TCE)	>18	Few days	Ozone precursor, secondary organic aerosol precursor
3	Ketones	>40	Few days	Ozone precursor, secondary organic aerosol precursor
4	Toluene	>200	Few hours to months	Ozone precursor, secondary organic aerosol precursor
5	Fluorinated compounds	>1000	>200 years	GWP-100 * = 135~17,400
6	N_2O	>3000	>100 years	GWP-100 = 273
7	NH_3	>250	Few hours	Fine particle precursor
8	HCl	>2000	Hours	Acid source, secondary organic aerosol formation

* GWP-100: 100-year time horizon global warming potential.

Since VOCs and greenhouse gases (e.g., fluorinated compounds and N_2O) demonstrate significant emission levels from semiconductor industries (Table 1), the continuous monitoring of these compounds is an important issue for environmental management. However, the process of monitoring VOCs and greenhouse gases that are emitted from semiconductor industries is still being developed [8–12].

In terms of continuous air monitoring, it is well known that the moisture content, including both gas and liquid phases, can have a significant effect on the bias of the monitoring process using gas analyzers [13–22], especially at high moisture contents due to the use of scrubbers in the semiconductor industry [12,23]. To mitigate moisture interference, moisture pretreatment devices (MPDs) are necessary. However, the potential loss of target analytes due to MPD usage is a crucial concern [13,14,17–22].

MPDs generally include condensation- and permeation-based devices [13,24]. Condensation-based MPDs utilize solid-phase condensation, with KPASS acting as a representative MPD; liquid-phase condensation uses coolers as representative MPDs [13,14,17–22]. Permeation-based MPDs operate based on the separation of H_2O and other compounds via a membrane; the Nafion^{TM} dryer is a representative MPD [13,14,17–22]. The basic structures of these MPDs are shown in Figure 1.

Studies have shown that condensation-based MPDs can result in a 10% loss of ozone at 30% relative humidity (RH) and a 40% loss at 80%RH. Similarly, SO_2 losses of 19.3%, 29.3%, and 61.5% have been observed at RH levels of 30%, 50%, and 80%, respectively, when a cooler was used for moisture removal [14,17,20]. It was reported that isobutyl alcohol, methyl isobutyl ketone, butyl acetate, and styrene experienced losses of approximately 19%, 4%, 5%, and 10%, respectively, at 80%RH, with concentration reproducibility varying from 8% to 31% [21]. This suggests that water within the cooler absorbs and desorbs analytes [21]. Additionally, HCl losses of up to 95% due to coolers have been reported [18].

Permeation-based MPDs are also commonly used for humidity control [13,24]. However, Nafion™ dryers have been found to introduce measurement errors, such as a 2 ppbv discrepancy when used with an ozone analyzer measuring 330 ppbv of O_3 [25]. These dryers also contribute to analyte loss; for example, H_2S losses of up to 7% at 100%RH [26]

and dimethyl sulfide losses of 10% at 13 ppbv and 100%RH [26] or 2% at 4.9 ppbv and 90%RH [27] have been documented. Notably, isobutanethiol exhibited a loss of up to 29% at 1.6 ppbv and 92%RH [27]. Significant VOC losses, including methyl ethyl ketone and isobutyl alcohol, have also been reported when using Nafion™ dryers [19,21,22].

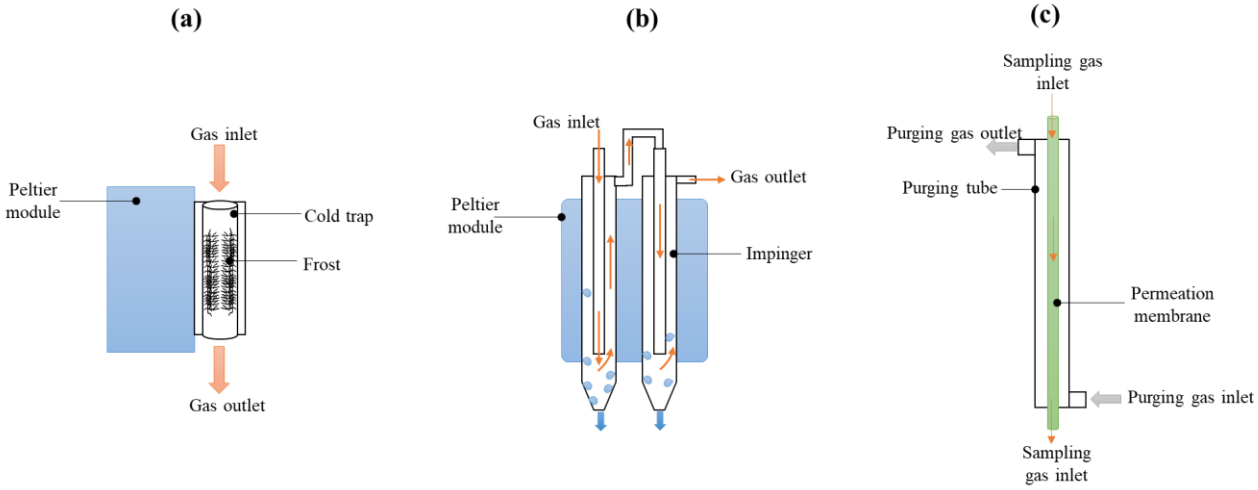


Figure 1. General schematic of moisture pretreatment devices for continuous emission monitoring: (**a**) KPASS; (**b**) cooler; and (**c**) Nafion™ dryer.

The studies of MPDs for VOCs have been well documented [19,21,22]. However, these studies were conducted with flow rates of less than 1 L/min and with aldehydes, ketones, and aromatic hydrocarbons [19,21,22]; halogenated hydrocarbons have not been considered. In terms of F compounds and N_2O, there is a lack of studies on MPDs for monitoring these compounds. On the other hand, gas analyzers for the continuous measurement of air pollutants commonly use flow rates around 1 L/min [28–31]. Therefore, MPDs have been widely recommended to be used with flow rates of 1 L/min [14,17,18,20]. However, for these greenhouse gases, the measurement process needs higher flow rates [12,32–34], which may cause overloading for conventional MPDs. Therefore, the investigation of MPDs at high loading capacities is necessary for monitoring VOCs and greenhouse gases emitted from semiconductor industries. Among the VOCs of concern, benzene, toluene, ethylbenzene, xylene, styrene, and ketones have been studied elsewhere [19,21,22]. In terms of greenhouse gases, N_2O has the highest water solubility [35–39]. Therefore, TCE was selected as a representative VOC, and N_2O was selected as a representative greenhouse gas emitted from semiconductor industries in order to assess the performance of MPDs on the measurement of VOCs and greenhouse gases. If the selected MPD could operate well with respect to TCE and N_2O, it could also operate with other VOCs and greenhouse gas compounds.

Consequently, this study aims to investigate the impact of MPDs on the measurement accuracy of TCE and N_2O at normal and high loading capacities. The findings will help identify the most suitable MPD techniques for accurately quantifying these pollutants in emissions from semiconductor manufacturing facilities.

2. Materials and Methods

2.1. Experimental Apparatus

A cooler (TC-Standard 6122, Bühler Technologies GmbH, North Rhine-Westphalia, Germany) was used as a representative liquid-based condensation method. A Nafion™ dryer with a 3 m length (SWG-A01-36/KF, AGC Inc., Tokyo, Japan) was used as a representative permeation method. On the other hand, KPASS (NSP-D, Nara Control, Seoul,

Republic of Korea), a recently developed MPD based on the frost filter approach [20,22], was used for comparison. The specifications of the used MPDs are shown in Table 2.

Table 2. Specifications of moisture pretreatment devices in the current study.

No.	Device	Code	Moisture Removal Mechanism	Basic Setup	Flow Rate (L/min)
1	Cooler	MPD_C	Liquid condensation	Condensation temperature: 2 °C	1~2
2	Nafion^{TM} dryer	MPD_N	Membrane permeation	Dry air/sample ratio: 4/1	1~2
3	KPASS	MPD_K	Frost filter	Supercooling	1~5

TCE was analyzed using a GC/FID (7200A, DS Science Inc., Gwangju-si, Republic of Korea). The GC/FID operation conditions are shown in Table 3. A 60 m capillary column with a diameter of 0.32 μm (DB 624, Agilent Technologies, Inc., Santa Clara, CA, USA) was applied for the GC. The TCE calibration curve is shown in Figure 2. The method detection limit for TCE was 0.44 ng.

Table 3. Operation conditions of GC/FID for TCE analysis.

Parameter	Unit	Value
Initial oven temperature (holding time)	°C (min)	80 (2)
Temperature ramp rate	°C min^{-1}	25
Final oven temperature (holding time)	°C (min)	120 (0.5)
Detector temperature	°C	280
Column flow rate	(mL/min)	1.5
Split ratio	-	20

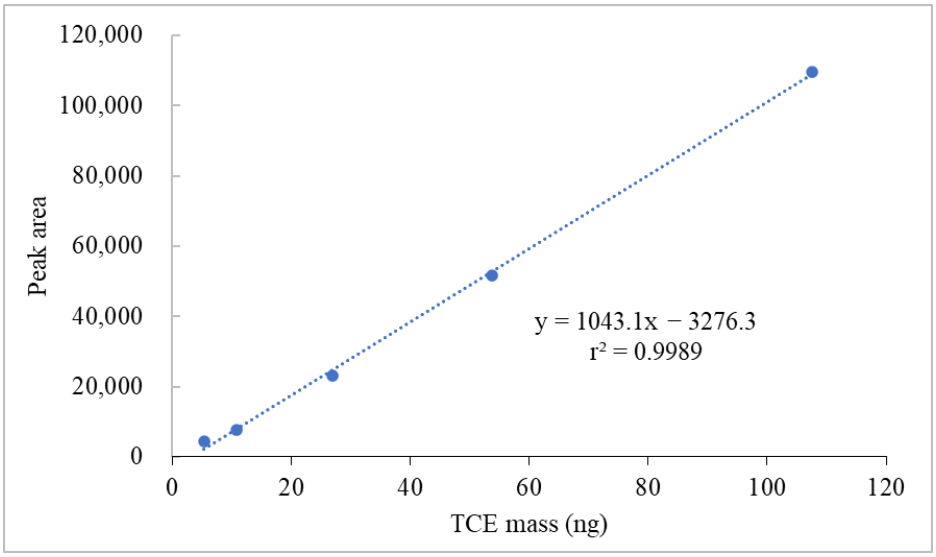


Figure 2. Calibration curve of GC/FID for TCE.

N_2O was analyzed using an IR spectroscopy analyzer (FGA5000, ELT Sensor, Bucheon-si, Republic of Korea). The measurement range of the analyzer was 0–20,000 ppm, with a resolution of 1 ppm and a detection limit of 10 ppm. Before use, the analyzer was calibrated with zero and span gases, as recommended by the manufacturer. In terms of humidity, a humidity sensor (Testo 645, Testo SE & Co. KGaA, Titisee-Neustadt, Germany) was used to measure the humidity in the sample gas.

2.2. Experimental Materials

TCE (100 ppm, Rigas, Daejeon, Republic of Korea) and N_2O (20,000 ppm, Rigas, Daejeon, Republic of Korea) were used as standard gases for the experiment. N_2 (99.99%) was used as the zero gas for calibrating the analyzer, as well as for diluting the standard gas.

2.3. Experimental Procedure

2.3.1. Investigation into the Humidity Effect on the Analytical Results of TCE and N_2O

Gas chromatography (GC) techniques, coupled with flame ionization detectors (FIDs) or mass selective detectors (MSDs), are widely used for analyzing TCE in air [40]. For N_2O, GC with an electron capture detector (ECD), the IR spectroscopy approach (e.g., Fourier-transform infrared spectroscopy (FTIR) and non-dispersive infrared (NDIR) spectroscopy), and cavity ring-down spectroscopy (CRDS) are commonly employed [41]. Among these, FTIR and IR spectroscopy are preferred for real-time N_2O monitoring [12,41]. However, both GC-based techniques and IR spectroscopy can be affected by the humidity in the sample gas [13,15,16,19,21,42–44]. In semiconductor manufacturing plants, wet scrubbers are widely used for pollutant removal [12], leading to high moisture content in the flue gas, which may introduce bias in the measurement of TCE and N_2O. Therefore, the effect of humidity on the measurement of TCE using GC/FID, as well as the measurement of N_2O using IR spectroscopy, was investigated to contribute more evidence to the existing body of literature. The experimental setup is presented in Figure 3.

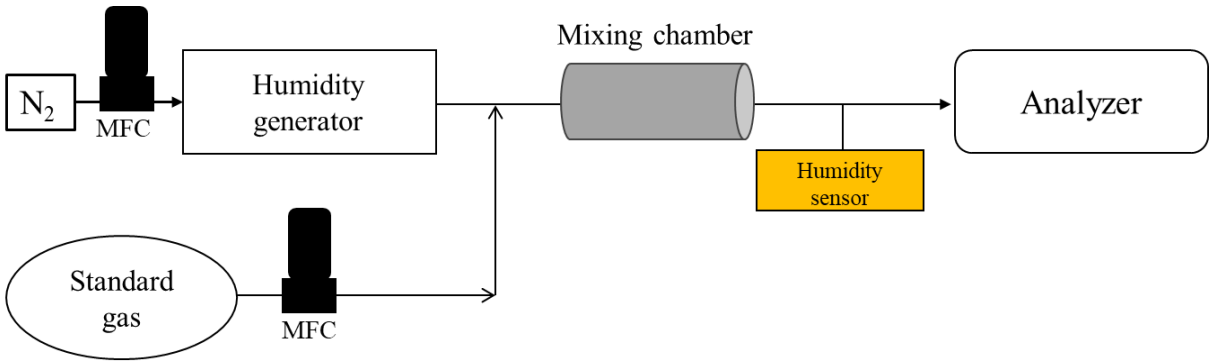


Figure 3. Experimental setup for humidity effect on TCE and N_2O analytical results.

In terms of TCE, the TCE standard gas was mixed with moist air to generate 50 ppm TCE at various humidities. The relative humidity (RH) of the sample varied from 10% to 90%. TCE was analyzed using GC/FID, and TCE samples were collected after the mixing chamber stage using a syringe. The injection volume of TCE into the GC/FID was 200 µL. For N_2O, the target concentration was 8500 ppm, and the humidity variations were the same as in the TCE experiment. After thorough mixing in the mixing chamber, N_2O concentrations were measured using the FGA5000 analyzer. A ten-minute average of the N_2O data was evaluated for each experiment. The relative mean squared error (RMSE), mean normalized error (MNE), and mean normalized bias (MNB) were calculated to assess the error of the analyzer compared to the standard gas. Details of the calculation method can be found elsewhere [45–48].

2.3.2. Investigation into the Performance of Moisture Pretreatment Devices at Normal Loading Capacities

Gas analyzers for the continuous measurement of air pollutants commonly use flow rates around 1 L/min [28–31]. Therefore, MPDs have been widely recommended to be used with a flow rate of 1 L/min. The performance of the MPDs of concern was investigated under a normal loading capacity with a 1 L/min flow rate.

Comparison of the Moisture Removal Efficiency with Respect to Various Moisture Pretreatment Devices at Normal Loading Capacities

Moisture removal efficiencies were investigated with respect to different MPDs. The experimental setup is presented in Figure 4.

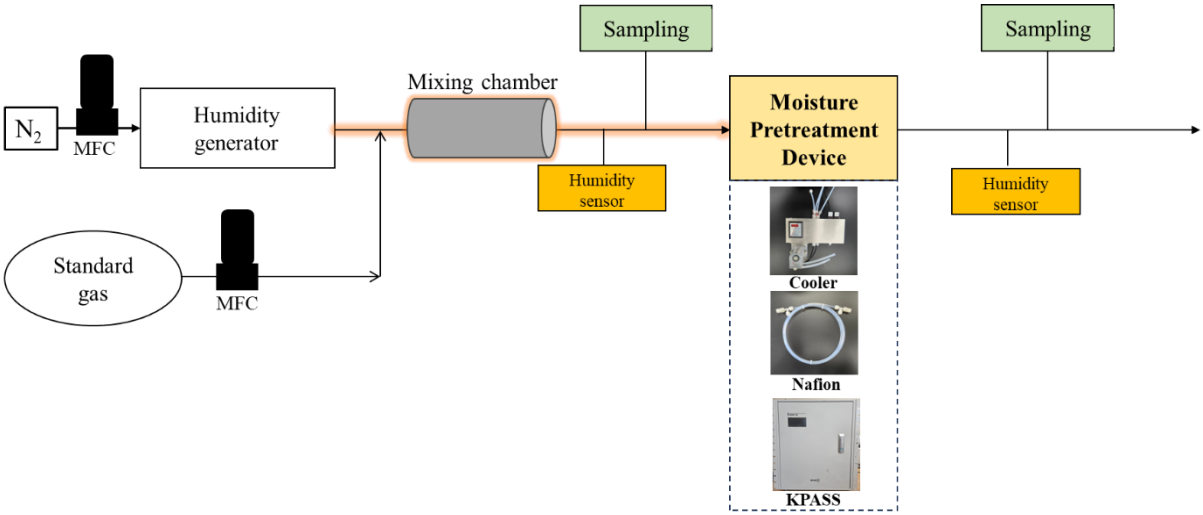


Figure 4. Experimental setup for performance tests of moisture pretreatment devices.

Room temperature conditions (25 °C, 90%RH) and stack conditions (150 °C, 20%v/v humidity) were used to investigate the moisture removal efficiencies of MPDs. The air flow rate was 1 L/min. For the moisture removal experiment, only humid air from the humidity generator, using the bubbling method, was introduced into the MPDs. Each MPD was warmed up for 10 min, and its respective performance was investigated for 10 min. Triplicate experiments were conducted.

Investigation into TCE and N_2O Recovery Rates with Respect to Different Moisture Pretreatment Devices at Normal Loading Capacity

The recovery rates of TCE and N_2O after passing through MPDs were investigated. The experimental setup is the same as shown in Figure 4. For TCE, 0.5 ppm and 50 ppm concentrations were generated under room and stack conditions. Due to the exposure limit of TCE, the maximum concentration of 50 ppm was selected, as shown in Table 4 [40].

Table 4. Time-weighted average exposure limit of TCE in several countries [40].

No.	Country	Exposure Limit (ppm)
1	USA	100
2	UK	100
3	Japan	50
4	Republic of Korea	50

For N_2O, a high concentration of 10,000 ppm was chosen based on emission levels at semiconductor facilities before treatment [23], and a low concentration of 100 ppm was selected due to its hazardous level [41]. The recovery rate of the analyte is calculated as shown in Equation (1).

$$Rec = \frac{(C_{in} - C_{out})}{C_{in}} \times 100 \quad (1)$$

Here, Rec is the recovery rate of the analyte (%), C_{in} is the initial concentration of the analyte (ppm), and C_{out} is the concentration of the analyte after passing the water pretreatment device (ppm).

As shown in Figure 4, one MPD was used in each experiment. For TCE, TCE samples were collected at sampling points and injected into the GC/FID for analysis. However, due to the effect of humidity on the analytical results, the initial concentrations of TCE were demonstrated under dry conditions. Afterward, humid air was mixed with the TCE standard gas at the same mixing ratio to maintain a consistent inlet concentration for the MPD performance test. The collected volume was also 200 μL. Similarly, N_2O concentrations were measured using the FGA5000 analyzer, which was connected to the sampling points. Initial N_2O concentrations were measured under dry conditions because the analyzer cannot operate at high humidity levels. When humid air was mixed to investigate the recovery rate, the analyzer was only connected to the sampling points after the MPDs. A ten-minute average of the data was used for comparison.

2.3.3. Investigation into the Performance of Moisture Pretreatment Devices at High Loading Capacities

For the air pollution monitoring of semiconductor industries with various emission gases, Fourier-transform infrared spectroscopy (FTIR) and quadrupole mass spectrometry (QMS) have been utilized [12]. Contrary to the conventional gas analyzer, the necessary flow rate of the system is recommended to be 4 L/min in order to balance response time and sensitivity [12,32–34]. Therefore, the performance of the MPDs was also investigated under a high loading capacity with a flow rate of 4 L/min.

Investigation into the Moisture Removal Efficiency of Various Moisture Pretreatment Devices at High Loading Capacities

The experimental setup and humidity conditions were the same as reported in a previous section (Comparison of the Moisture Removal Efficiency with Respect to Various Moisture Pretreatment Devices at Normal Loading Capacities). However, the air flow rate was 2 L/min and 4 L/min. The performance of each MPD was also investigated for 10 min. Each experiment was repeated 3 times.

Improvement in the Performance of Moisture Pretreatment Devices

After investigating the performance of MPDs with respect to a flow rate of 4 L/min, it was found that MPD_N and MPD_C could not operate well at flow rates of 4 L/min and at a high inlet gas temperature (see Section 3.3.1). In contrast, although MPD_K could operate at high flow rates and high temperatures, the humidity removal efficiency was lower than 80%. Therefore, MPDs should be improved to achieve better performance. More membranes could be used to reduce the flow distribution to each one; however, the investment price will be much higher. For MPD_C, its improvement is unnecessary because its analyte recovery was lower than that of the other MPDs. Therefore, the improvement in MPD_K was the most successful. Due to the higher flow rates, the residence time of the sample gas in MPD_K is shorter. Thus, to improve the residence time, larger volumes of the cold trap in MPD_K should be taken into account. To increase the volume, three designs of cold traps were simulated, as shown in Figure 5.

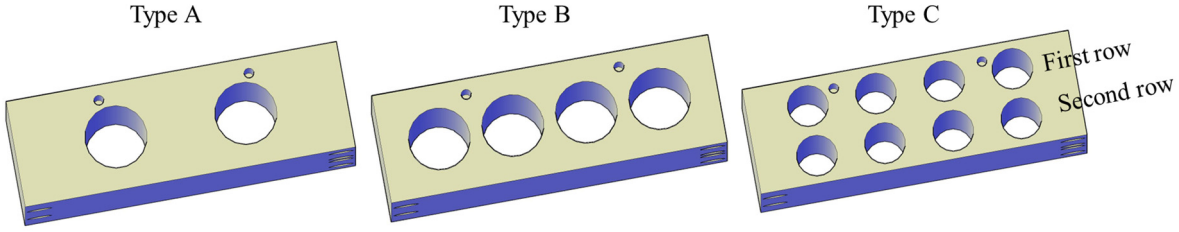


Figure 5. Various types of cold traps for MPD_K.

Type A, which is the original cold trap design, consists of two three-quarter-inch pipes. Type B is a new design with four three-quarter-inch pipes, and Type C consists of eight half-inch pipes (arranged in a 4 × 2 array over two rows). Their length was identical, at 8 cm. For these three different flow paths, the cooling efficiency was theoretically analyzed in terms of the heat exchange area, residence time, and temperature homogeneity based on Fourier's law and the Graetz number in order to figure out the optimal configuration. The heat exchange area refers to the surface area through which heat transfer occurs and is a critical factor that determines the efficiency of thermal exchange [49]. The heat exchange areas were calculated based on Equation (2).

$$A = \pi \times D \times L \times N \tag{2}$$

Here, A is the total heat exchange area (cm^2), D is the diameter of the pipe (cm), L is the length of the pipe (cm), and N is the number of pipes.

Residence time refers to the duration that the fluid remains inside the pipe, which is a critical factor in determining how effectively the gas can be cooled [50]. Under the same flow rate conditions, a longer residence time allows for an increased opportunity for heat exchange, increasing the likelihood of achieving lower temperatures. In this study, the residence time for each structure was calculated using Equation (3).

$$t_s = \frac{N \times A_c \times L}{Q} \tag{3}$$

Here, t_s is the residence time (s), N is the number of pipes, A_c is the section area of the pipe, L is the pipe length (m), and Q is the air flow rate (m^3/s).

Fourier's law is a fundamental principle that describes conductive heat transfer and is used to predict temperature distribution across the cross-section of a pipe [51]. It determines how heat is transferred through the pipe wall and how temperature is distributed in the cross-sectional direction. As concerns Type C, where the Peltier element is installed on only one side, the cooling effect on the opposite side of the flow path is likely to be significantly weaker. This can act as a factor that reduces the temperature homogeneity within the pipe. Heat flux, based on Fourier's law, was calculated based on Equation (4).

$$q = -k \times \frac{\Delta T}{\delta} \tag{4}$$

Here, q is the heat flux (W/m^2), k is the thermal conductivity of the materials (W/m·K) (k = 237 W/m·K for aluminum), ΔT is the temperature difference between two points (K), and δ is the heat transfer distance (m).

The Graetz number (Gz) is a dimensionless parameter that indicates how effectively heat is transferred from the pipe wall to the center of the fluid; it serves as an important criterion for evaluating heat exchange efficiency [52]. The Graetz number (Gz) was defined using Equation (5), as follows:

$$Gz = \frac{D}{L} \times Re \times Pr \tag{5}$$

where D is the diameter of the pipe (m), L is the pipe length (m), Re is the Reynolds number, and Pr is the Prandtl number.

After a theoretical comparison of the three types of cold traps, a practical comparison was conducted by attaching each cold trap to the MPD_K to investigate its moisture removal efficiency and analyte recovery rates. The air flow rate was 4 L/min. High concentrations of TCE and N_2O were selected for this experiment. The experimental setup is the same as that depicted in Figure 4. The performance was investigated for 10 min. Triplicate experiments were conducted. Finally, the optimal design was selected.

All data were analyzed using Excel (Version 2501, Microsoft Corporation, Redmond, WA, USA). A *t*-test was conducted using MATLAB software (Version 9.10.0.1684407, MathWorks, Inc., Natick, MA, USA).

3. Results and Discussion

3.1. Effect of Humidity on the Analytical Results of TCE and N_2O

The effect of humidity on the TCE analytical results using GC/FID is shown in Figure 6.

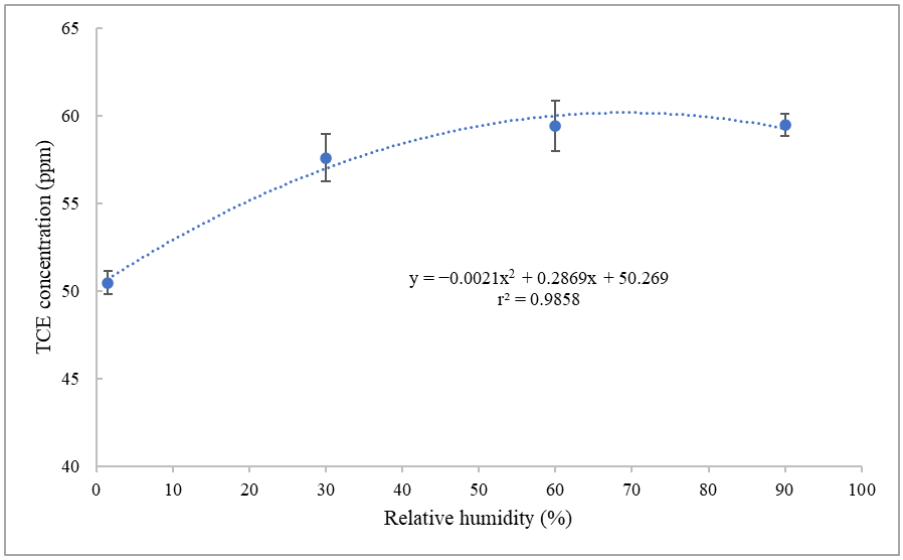


Figure 6. Relationship between the humidity of the gas samples and the TCE analytical results using GC/FID (error bar is the standard deviation).

As shown in Figure 6, the analytical results were approximately 50 ppm when the dry samples were analyzed. However, when the humidity in the sample increased, the analytical TCE concentrations significantly increased. A *t*-test between the mean TCE concentrations under dry and humid conditions showed a significant difference with a 95% confidence interval, due to *p*-values < 0.05. RMSE, MNE, and MNB were 0.72 ppm, 1.1%, and 0.97% under dry conditions; however, they increased to 9.47 ppm, 18.9%, and 18.9% at 90%RH. Therefore, humidity caused significant errors in the analytical results. Accordingly, the humidity in the sample can significantly bias the TCE analysis when using GC/FID. The effect of humidity on the measurement of VOCs has also been reported elsewhere. It was found that when VOC samples with 85%RH at 30 °C were analyzed using GC/FID, the analytical errors varied from 3% to 11.9%. In particular, the errors for chloroform compounds such as 1,2,4-trichlorobenzene and o-dichlorobenzene were 8.2% and 3%, respectively [42]. The measurement error for benzene using GC/FID was reported to be as high as 21% when the sample had 80%RH at 20 °C [53]. Therefore, the moisture content in the sample gas should be reduced when using GC/FID [53].

In terms of N_2O, the effect of humidity on the N_2O analyzer based on IR spectroscopy is presented in Figure 7.

As shown in Figure 7, humidity also caused significant errors in the measurement of N_2O using IR spectroscopy. RMSE, MNE, and MNB were found to be 200 ppm, 2.5%, and 2.49% at 10%RH, but were reported as 1890 ppm, 22.2%, and 22.25% at 90%RH. This indicates the significant positive errors of the analytical results. Humidity interference was generally observed in IR spectroscopy analyzers because H_2O spectra often overlap with the spectra of other compounds in the mid-IR region [15,16,44]. Therefore, humidity removal is necessary to improve the measurement accuracy of IR spectroscopy analyzers.

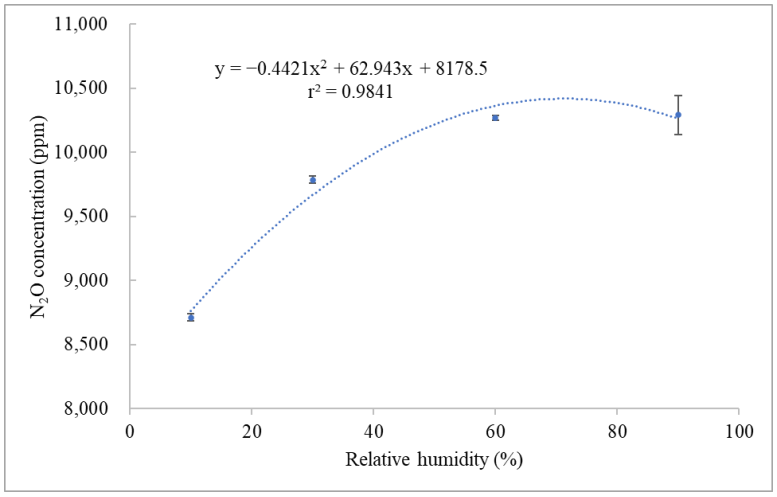


Figure 7. Relationship between the humidity of the gas samples and the N_2O measurement results using IR spectroscopy (error bar is the standard deviation).

3.2. Comparison of the Performance of MPDs with Respect to Normal Loading Capacities

3.2.1. Comparison of the Moisture Removal Efficiency of Different MPDs at Normal Loading Capacities

The moisture removal efficiencies of MPD_K, MPD_N, and MPD_C at room and stack conditions are depicted in Figure 8.

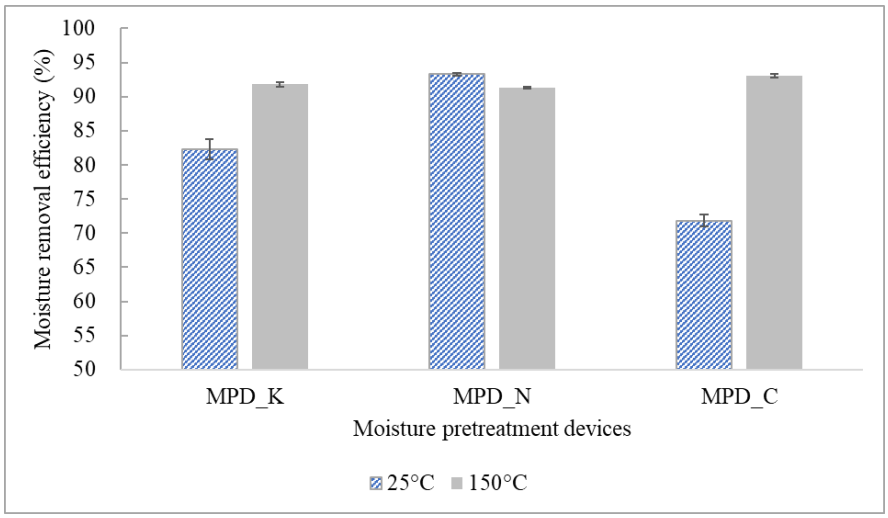


Figure 8. Moisture removal efficiencies of various moisture pretreatment devices with respect to room and stack conditions at normal loading capacities.

As shown in Figure 8, MPD_N exhibited the best moisture removal efficiencies under both conditions, followed by MPD_K and MPD_C. MPD_C showed the lowest moisture removal efficiency because moisture was removed by condensation at the dew point of water. The moisture removal efficiency under stack conditions was higher than that under room conditions because the sample at stack conditions contained more moisture than the sample at room conditions. The moisture removal efficiency pattern among various MPDs was found to be similar to that in another study (Table 5). As shown in Table 5, the cooler showed a lower moisture removal efficiency than the other MPDs, especially at room temperature. At high-temperature conditions, all MPDs revealed over 90% moisture removal efficiency. Consequently, Nafion™ dryers and KPASS are recommended for effective moisture control in gas analysis at room temperature. At high temperatures, all MPDs are appropriate for the removal of moisture in the sample gas.

Table 5. Comparison of the moisture removal efficiency of various moisture pretreatment devices.

No.	Target Analyte	Condition	Average Moisture Removal Efficiency (%)		
			KPASS	Nafion	Cooler
1	VOCs [21]	25 °C, 90%RH	90	-	60
2	VOCs [19]	25 °C, 90%RH	-	96	67
3	O_3, SO_2, and CO [17]	25 °C, 80%RH	93	-	59
4	O_3 and SO_2 [20]	25 °C, 30~80%RH	87~95	85~90	
5	VOCs [22]	25 °C, 90%RH	89	71	95
6	TCE and N_2O (this study)	25 °C, 90%RH	82	93	72
7	TCE and N_2O (this study)	150 °C, 20%v/v	92	91	92

3.2.2. Effect of Moisture Pretreatment Devices on the Recovery of TCE and N_2O at Normal Loading Capacities

The TCE recovery rates with respect to various MPDs at room and stack conditions are presented in Figure 9.

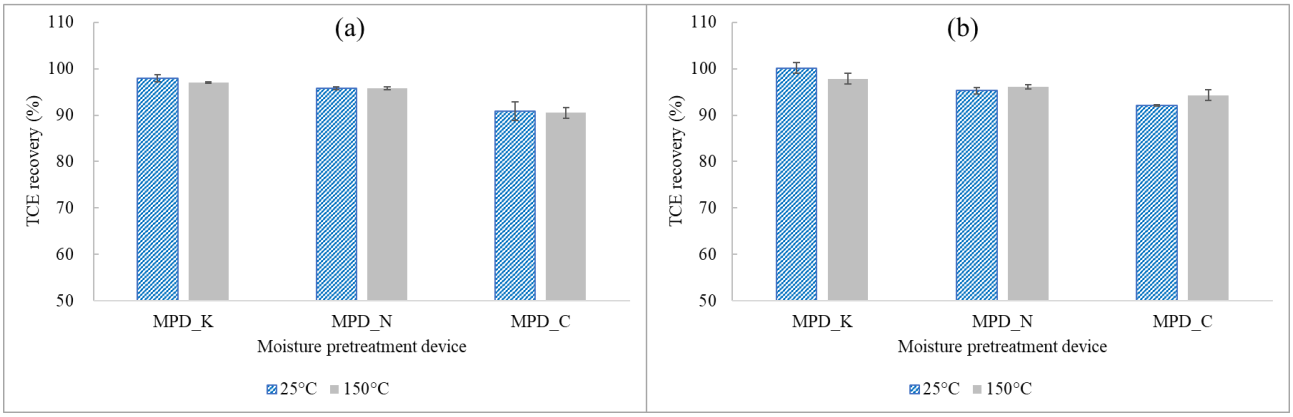


Figure 9. TCE recovery rates with respect to various MPDs and conditions at (**a**) 0.5 ppm TCE and (**b**) 50 ppm TCE.

As shown in Figure 9, MPD_K revealed the highest TCE recovery rates (>97%) at both high and low concentrations. In contrast, MPD_C showed the lowest TCE recovery rate, as it removes moisture in the liquid phase, which can capture TCE due to its water solubility of 1.28 g/L at 25 °C [54]. Although MPD_N demonstrated a better moisture removal efficiency, it resulted in a higher loss of TCE compared to MPD_K. This loss may be attributed to the deposition of TCE on the inner membrane of MPD_N, which has a length of 3 m, leading to a retention time of over 2 s. In contrast, the retention time of TCE in MPD_K was only approximately 0.06 s. Thus, the TCE loss in MPD_N might be higher than in MPD_K.

In terms of N_2O, the recovery rates with respect to different MPDs are depicted in Figure 10.

As shown in Figure 10, MPD_C exhibited the lowest N_2O recovery rates. Since the water solubility of N_2O is 1.2 g/L at 20 °C [55], it could be captured by water droplets in MPD_C. Both MPD_K and MPD_N demonstrated high recovery rates for N_2O, with MPD_K achieving approximately 100% recovery under both room and stack conditions, while MPD_N showed a slightly lower recovery rate. However, both MPD_K and MPD_N performed significantly better than MPD_C. This suggests that MPD_K and MPD_N are more suitable for N_2O measurement in terms of recovery efficiency.

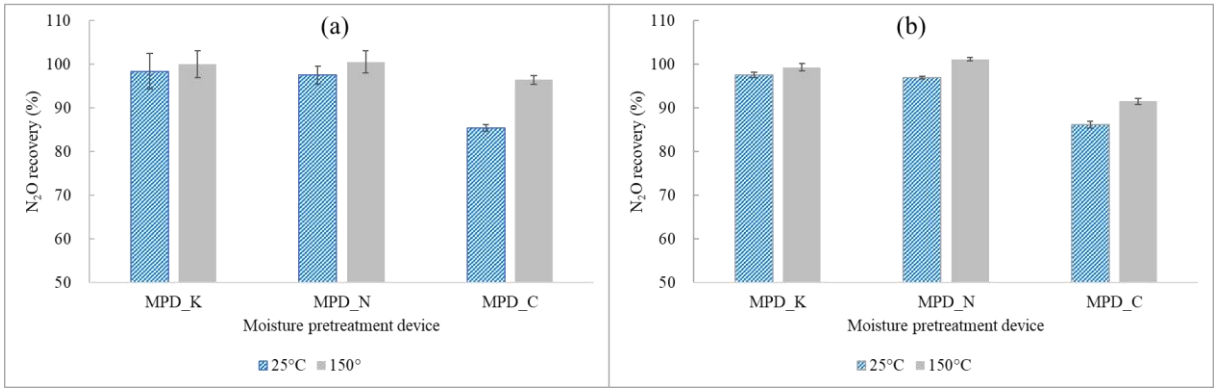


Figure 10. N_2O recovery rates with respect to various MPDs and conditions at (**a**) 100 ppm N_2O and (**b**) 10,000 ppm N_2O.

To clarify the effectiveness of MPDs on the analytical errors of the analytical process, RMSE, MNE, and MNB were calculated between measurement data when using MPDs and standard gas concentrations; these values were compared to those obtained in Section 3.1. The calculated results are presented in Table 6.

Table 6. Comparison of analytical errors with and without the use of MPDs.

Condition	N_2O			TCE		
	RMSE (ppm)	MNE (%)	MNB (%)	RMSE (ppm)	MNE (%)	MNB (%)
With MPD at 25 °C	131	1.3	−1.3	0.46	0.79	0.15
With MPD at 150 °C	238	2.3	2.3	1.13	1.95	−1.95
Direct wet sample at 90%RH	1889	22.2	22.2	9.47	18.9	18.9

As shown in Table 6, when an MPD_K was applied, the errors were less than 2.3% for N_2O and less than 2% for TCE. In contrast, when the 90%RH sample was analyzed, the bias was high, and the errors were over 22% for N_2O and over 18% for TCE. This is clear evidence that suggests MPDs help to improve the measurement errors.

3.3. Comparison of the Performance of MPDs with Respect to High Loading Capacities

3.3.1. Comparison of the Moisture Removal Efficiency of Different MPDs with Respect to High Loading Capacities

The moisture removal efficiencies of MPDs with respect to various flow rates at 25 °C and 150 °C are presented in Figure 11.

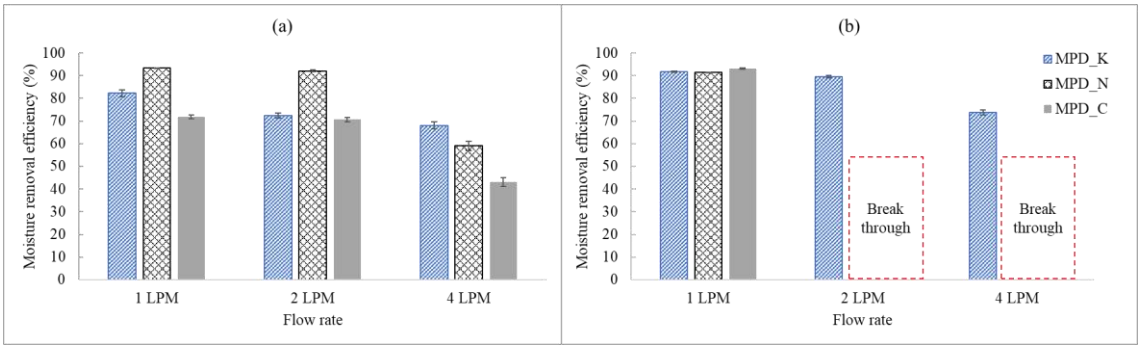


Figure 11. Moisture removal efficiencies of MPDs with respect to various conditions (**a**) at 25 °C and (**b**) at 150 °C.

As shown in Figure 11, all devices exhibited high removal efficiencies at a flow rate of 1 L/min. However, as the flow rate increased, moisture could not be effectively removed at 2 LPM and 4 LPM conditions when the gas temperature was 25 °C. In particular, both MPD_N and MPD_C showed breakthroughs at 150 °C, while MPD_K also showed a lower moisture removal efficiency at 4 L/min. For MPD_C and MPD_K, at low flow rates (1 LPM), longer residence times ensure a higher removal efficiency. At 4 LPM, the gas passes through too quickly, preventing condensation and resulting in moisture being discharged without removal. In terms of MPD_N, Nafion^{TM} membranes should be operated below 80 °C, as structural deformation may occur at higher temperatures. However, in this experiment, the inlet gas temperature exceeded 100 °C, surpassing the membrane's allowable limit. Consequently, a temperature differential occurred between the membrane's interior and exterior, leading to rapid internal cooling and the condensation of water vapor into liquid droplets. Since the Nafion^{TM} dryer is designed to remove water in gaseous form, the presence of a large amount of condensed moisture inside the membrane can significantly reduce its dehumidification performance. Despite increasing the purge gas flow to facilitate moisture removal, dehumidification was unsuccessful, likely because the condensed water inside the membrane blocked vapor movement, hindering proper drying. Although purge gas normally helps expel moisture from the membrane, the presence of liquid water prevents vapor diffusion through the membrane and inhibits the purge gas from directly removing water droplets. As a result, inefficient purge gas flow can form internal pressure differences, causing gas backflow [56]. Moreover, even with increased purge gas flow, the gas blockage might have occurred due to non-uniform flow inside the membrane or residual condensed water that could not be quickly drained. Although a higher purge gas flow is expected to enhance moisture removal, in this case, fast-moving gas could not effectively remove the moisture clinging to the membrane surface and may have caused turbulence, which impeded condensate drainage. Consequently, MPD_K showed the highest potential for removing moisture at high loading capacities, although the efficiency decreased. To improve the removal efficiency, the residence time should be improved.

3.3.2. Optimal Cold Trap Design for MPD_K to Effectively Operate at High Loading Capacities

Theoretical Assessment of Various Cold Trap Designs

The theoretical heat transfer efficiency of three types of cold traps was simulated and is shown in Table 7.

Table 7. Specifications of Type A, Type B, and Type C cold traps.

Type	ID (cm)	Pipe Count	Total Volume (cm^3)	Residence Time (s)	Surface Area (cm^2)	Heat Flux (W/m^2)		Graetz Number	
						25 °C	150 °C	25 °C	150 °C
A	1.905	2	45.6	0.68	95.76	541,714	1,557,232	247.59	167.30
B	1.905	4	91.21	1.37	191.5	541,714	1,557,232	123.79	83.65
C	1.27	8	81.07	1.22	255.4	First row: 1,036,066 Second row: 366,831	First row: 2,978,689 Second row: 1,055,889	61.90	41.82

As shown in Table 7, Type C, having the highest number of pipes, shows the largest surface area (255.35 cm^2). Type B, with a larger pipe volume and a slower flow velocity, exhibited the longest residence time (1.37 s). In contrast, Type A, which has the smallest number of tubes and the smallest cross-sectional area, recorded the lowest values for both residence time (0.684 s) and surface area (95.76 cm^2). The cooling performance generally improves when the gas is in contact with a larger surface area of the tube wall and for a longer period of time. From this perspective, Type B has the advantage of providing a sufficient heat transfer time due to its long residence time, while Type C facilitates rapid heat exchange through its large surface area—each offering favorable characteristics for

effective cooling. Meanwhile, under high-flow conditions, both moisture removal efficiency and the recovery rate of target substances become important considerations. Compared to Type A, Type B has approximately twice the residence time and more than twice the surface area, which can significantly enhance moisture removal performance. However, a longer residence time also increases the likelihood of some substances being lost due to extended contact with the cooling surfaces. In contrast, although Type C has a shorter residence time than Type B, it is clearly longer than that of Type A, and it possesses the largest surface area among the three structures. As such, Type C may offer a balanced performance between recovery rate and moisture removal efficiency.

In terms of heat transfer distance, the shorter the heat transfer distance, the more rapidly the heat flux increases under the same material and temperature conditions. In particular, the first row of Type C exhibited a very high heat transfer performance, whereas the second row within the same structure shows a significant decrease in performance due to the longer heat transfer distance (Table 7). Types A and B had structurally identical heat transfer distances, resulting in the same heat flux values. These results highlight the critical importance of heat transfer distance as a physical factor in structural design and confirm its role as a key parameter for optimizing heat transfer efficiency. Additionally, as the inlet temperature of the gas increases, the temperature difference for heat transfer becomes larger, which further enhances the cooling efficiency of structures with shorter heat transfer paths. This characteristic is particularly evident in the first row of Type C, which recorded the highest heat flux under high-temperature fluid conditions, suggesting that it may serve as the most advantageous structure in terms of cooling efficiency.

Since a lower Graetz number generally indicates a more uniform temperature distribution across the pipe cross-section, Type C is the most advantageous in terms of cross-sectional heat transfer uniformity under both temperature conditions (Table 7). However, in Type C, four of the eight pipes are located farther from the thermoelectric element, resulting in a relatively longer heat conduction path. This increases the likelihood of delayed or uneven heat transfer. In contrast, Type B features all pipes evenly arranged along the same heat transfer path, providing the most favorable condition for uniform temperature distribution throughout the structure.

Accordingly, although Type C has the longest residence time and the largest heat exchange area—suggesting the highest heat transfer efficiency—it may suffer from the poorest temperature uniformity, potentially affecting the recovery rate. On the other hand, Type B, which uses multiple thicker pipes, offers a large overall heat exchange area, sufficient residence time, and consistent pipe placement along identical heat transfer paths. Therefore, it is expected to achieve an excellent balance between cooling efficiency and temperature homogeneity. These characteristics suggest that Type B is likely to deliver a stable cooling performance even under high-flow conditions.

Performance of the Modified MPD_K with Respect to Various Cold Trap Designs at High Loading Capacities

Three types of cold traps were used to investigate the moisture removal efficiencies at low and high temperatures. The experimental results are depicted in Figure 12.

As shown in Figure 12, under the 25 °C condition (a,b,c), all three types exhibited stable moisture removal behavior, and clear differences in removal performance were observed among the structures. Moisture removal efficiencies of Type A, Type B, and Type C were approximately 66.5%, 75.6%, and 83.6%, respectively. These results align with the general principle of heat transfer, in which moisture removal efficiency improves as residence time and heat transfer area increase. In particular, Type C has the largest number of flow paths and the greatest total heat exchange area. Although the inner diameter of each pipe is small, the high number of flow paths allows the flow velocity to be effectively dispersed, resulting

in a relatively long residence time. These structural characteristics contribute positively to enhanced cooling performance, which was reflected in the high moisture removal efficiency observed in the experiment. However, when the air temperature was 150 °C, the performance of the three types of cold traps was changed (Figure 12d–f). While Type C initially demonstrated an excellent moisture removal performance, condensate rapidly accumulated inside the device as the experiment progressed, eventually leading to saturation. Following this, a sharp increase in the humidity of the outlet air was observed, which was interpreted as the system reaching its moisture handling capacity due to the rapid condensation of a large amount of water in a short period under high-temperature conditions. Although Type C exhibited excellent short-term cooling performance, owing to its short heat transfer distance, small pipe diameter, and long residence time, with the cooling effect reaching deeply into the center of the pipe, its actual performance showed a temperature drop in the rear row, which is farther from the thermoelectric element, and the rapid accumulation of condensate within the structure led to saturation. Despite its strong cooling capacity, these findings reveal structural limitations in fluid discharge and condensate management, negatively affecting sustained moisture removal and recovery rates.

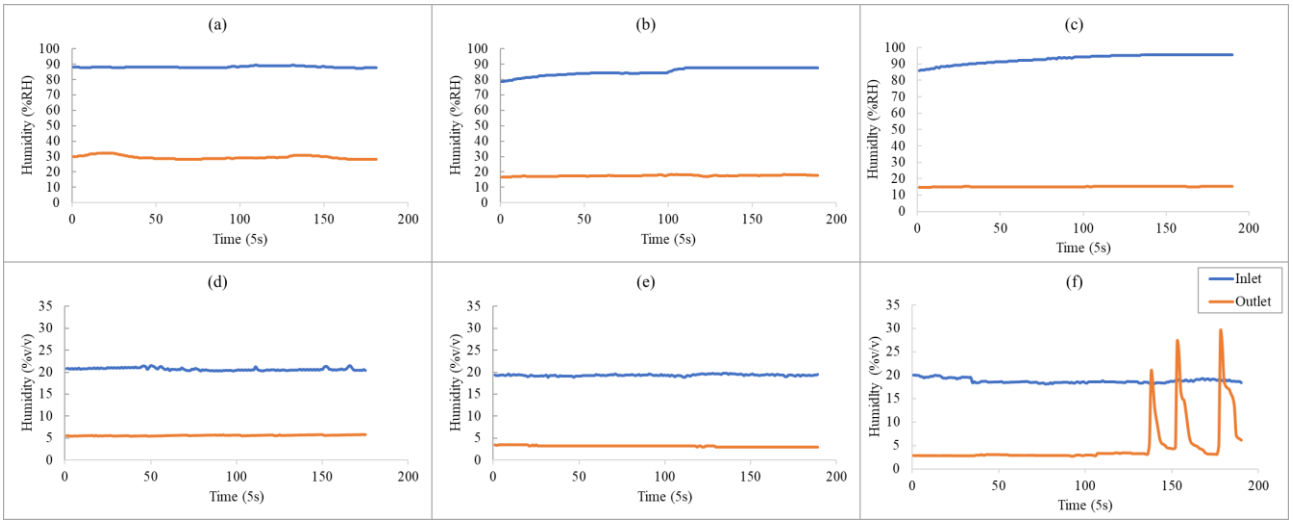


Figure 12. Inlet and outlet humidity of different types of cold traps at 25 °C for (**a**) Type A, (**b**) Type B, and (**c**) Type C, as well as at 150 °C for (**d**) Type A, (**e**) Type B, and (**f**) Type C.

In contrast, Type B maintained a stable moisture removal performance, even under high-temperature conditions, due to its relatively large heat transfer area, uniform temperature distribution, and steady flow dispersion. Throughout the experiment, the variation in removal efficiency was minimal, and no structural saturation occurred during prolonged operation. These results demonstrate that Type B is an optimal cold trap structure that is capable of maintaining both cooling performance and structural reliability under hot and humid conditions.

The recovery of TCE and N_2O with respect to Types A, B, and C is shown in Figure 13.

As shown in Figure 13, both Type B and C demonstrated higher recovery rates compared to Type A, with Type B particularly standing out due to its high average values and low standard deviations, indicating that it successfully balances moisture removal performance and analyte gas recovery stability. Although Type C was theoretically expected to deliver an excellent moisture removal performance due to its large heat transfer area and long residence time, the actual experiment showed that it rapidly removed moisture in the early stage, causing the structure to become quickly saturated. This characteristic is likely due to limitations in condensate handling capacity and moisture retention within the struc-

ture, which reduced heat exchange efficiency and ultimately increased the risk of analyte gas loss during prolonged operation. As a result, Type C exhibited a significant drop in TCE and N_2O recovery rates. In contrast, Type A, with its simple structure and short residence time, allowed the sample gas to pass through quickly, minimizing losses. Type B, on the other hand, achieved a well-balanced performance by maintaining strong moisture removal capabilities while avoiding condensate saturation or temperature imbalance, resulting in stable recovery rates. In particular, Type B maintained over 98% recovery under both temperature conditions while also demonstrating high moisture removal efficiency, making it the most suitable structure for ensuring the quantitative reliability of gas analysis. These results demonstrate that Type B achieves the most ideal balance among the three key design variables—heat transfer area, residence time, and temperature homogeneity—and, as such, successfully meets both objectives of moisture removal and gas preservation. Therefore, among the three structures proposed in this study, Type B is evaluated as the optimal pretreatment configuration in terms of both moisture removal efficiency and gas recovery stability under high-flow conditions.

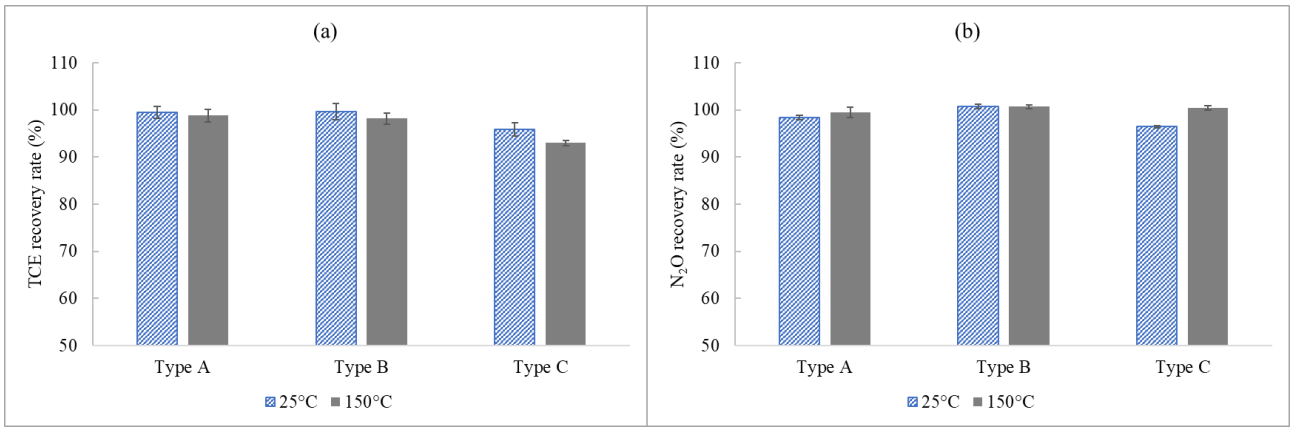


Figure 13. TCE (**a**) and N_2O (**b**) recovery rates with respect to various cold trap types.

Consequently, KPASS exhibited the best performance among the tested MPDs for removing moisture from TCE and N_2O samples at normal loading capacities. This pattern was consistent with previous studies (Table 8). In terms of high loading capacities, the Nafion^{TM} membrane and cooler revealed their limitation at high temperatures and high flow rates. In contrast, modified KPASS showed good moisture removal efficiency and analyte recovery rates with less investment. In particular, although the sample gas had high temperatures and flow rates, the modified KPASS still retained a high moisture removal efficiency. This removal efficiency was also comparable to previous studies (Table 8) that used conventional MPDs and flow rates of less than 1 L/min. The KPASS device removes more moisture than the cooler because it employs a frost-based filter, which captures more water vapor than liquid droplets [20]. Additionally, KPASS causes less analyte loss compared to Nafion™ due to the shorter retention time of analytes within the device. Furthermore, the modified KPASS device can operate at high sample gas temperatures and high flow rates, whereas high temperatures can damage the Nafion™ membrane. Therefore, KPASS is recommended for effective moisture control when analyzing TCE and N_2O. However, the current KPASS device uses a Peltier element to cool the cold trap, which consumes a significant amount of energy to maintain the desired temperature when high-temperature gas is introduced into the device. This leads to increased operating costs. Moreover, the performance of the Peltier element is sensitive to environmental conditions. High ambient temperatures, such as during the summer, can reduce the cooling efficiency of the Peltier, resulting in a decreased moisture removal efficiency. Consequently,

measurement errors may increase due to the higher outlet humidity. These limitations of the KPASS device should be taken into consideration.

Table 8. Recovery rates of analytes with respect to various moisture pretreatment devices.

No.	Compound	Condition	Flow Rate (L/min)	Average Recovery Rate (%)		
				KPASS	Nafion	Cooler
1	Methyl ethyl ketone [19,21]	25 °C, 80%RH, 100 ppb	0.2	103	7.5	100
2	Isobutyl alcohol [19,21]	25 °C, 80%RH, 100 ppb	0.2	96.6	21.4	91.7
3	Methyl isobutyl ketone [19,21]	25 °C, 80%RH, 100 ppb	0.2	99.5	1.47	94.4
4	Butyl acetate [19,21]	25 °C, 80%RH, 100 ppb	0.2	97.9	1.5	90.8
5	Styrene [19,21]	25 °C, 80%RH, 100 ppb	0.2	99.2	82.8	88.6
6	Benzene [22]	25 °C, 90%RH, 200 ppb	0.5	97	98	97
7	Toluene [22]	25 °C, 90%RH, 200 ppb	0.5	97	88	97
8	Ethylbenzene [22]	25 °C, 90%RH, 200 ppb	0.5	97	97	97
9	p-xylene [22]	25 °C, 90%RH, 200 ppb	0.5	98	97	96
10	Ozone [20]	25 °C, 80%RH, 100 ppb	1	97	94	-
11	SO_2 [17]	25 °C, 80%RH, 150 ppb	1	100	-	93
12	CO [17]	25 °C, 80%RH, 25 ppm	1	98	-	93.6
13	TCE (this study)	25 °C, 90%RH, 0.5 ppm	1	98	96	91
14	TCE (this study)	25 °C, 90%RH, 50 ppm	1	100	95	92
15	TCE (this study)	150 °C, 20%v/v, 0.5 ppm	1	97	96	90
16	TCE (this study)	150 °C, 20%v/v, 50 ppm	1	98	96	94
17	N_2O (this study)	25 °C, 90%RH, 100 ppm	1	98	98	85
18	N_2O (this study)	25 °C, 90%RH, 10,000 ppm	1	98	97	86
19	N_2O (this study)	150 °C, 20%v/v, 100 ppm	1	100	100	96
20	N_2O (this study)	150 °C, 20%v/v, 10,000 ppm	1	99	100	92
21	TCE (this study)	25 °C, 90%RH, 50 ppm	4	99.7	-	-
22	TCE (this study)	150 °C, 20%v/v, 50 ppm	4	98.2	-	-
23	N_2O (this study)	25 °C, 90%RH, 10,000 ppm	4	100.7	-	-
24	N_2O (this study)	150 °C, 20%v/v, 10,000 ppm	4	100.6	-	-

4. Conclusions

Various moisture pretreatment devices (MPDs) were evaluated for their ability to remove moisture from TCE gas samples analyzed using GC/FID, as well as N_2O gas samples measured using IR spectroscopy. The MPDs under investigation included a KPASS (MPD_K), a Nafion™ dryer (MPD_N), and a cooler (MPD_C). The moisture removal efficiencies and analyte recovery rates were assessed under both room and stack conditions for TCE and N_2O gases at normal loading capacities and high loading capacities. The effects of humidity on the measurement errors of TCE using GC/FID and N_2O using IR spectroscopy were also examined. The results indicated that moisture content had a significant impact on the analytical accuracy of TCE using GC/FID and on the measurement of N_2O using IR spectroscopy. In terms of normal loading capacity, when the MPDs were used to remove moisture from the gas samples, the average moisture removal efficiencies of MPD_K, MPD_N, and MPD_C were 82%, 93%, and 72%, respectively, under room conditions, and 92%, 91%, and 92%, respectively, under stack conditions. Regarding TCE recovery rates, MPD_C resulted in less than 95% recovery across all conditions, whereas MPD_K and MPD_N achieved over 95% recovery in all cases, with MPD_K demonstrating the highest TCE recovery rate. For N_2O, MPD_C exhibited the lowest recovery rates (85–96%), while MPD_K and MPD_N maintained recovery rates above 97% across all conditions. However, all conventional MPDs did not operate well at high loading capacities. The Nafion™ dryer and cooler did not work properly at a high temperature (150 °C) and flow rate (4 L/min). In terms of the KPASS device, the original design did not achieve an acceptable moisture removal efficiency. However, when a new cold trap structure was developed to achieve the high loading capacity with the least investment, it was found that the recovery rate of the modified KPASS was over 98% and the moisture removal efficiency was over 85%. Consequently, a moisture pretreatment device should

be used to remove moisture from the gas samples when analyzing TCE using GC/FID and measuring N_2O using IR spectroscopy to minimize analytical bias due to humidity. When selecting an MPD, a frost-based device is recommended to ensure both effective moisture removal and high analyte recovery rates for TCE and N_2O. Since this approach is applicable to TCE and has previously been found to be suitable for aromatic hydrocarbons, aldehydes, and ketones, the frost-based moisture pretreatment device can be applied for the measurement of VOCs emitted not only from semiconductor industries but also from other major sources. This approach also demonstrated a good performance with N_2O, which has the highest loss potential during the condensation process among greenhouse gases due to its high water solubility. Therefore, this method can be employed for monitoring greenhouse gases emitted from the semiconductor or electrical industries, which have similar emission patterns of gases with high global warming potential. However, due to the limitations of using Peltier elements for the cooling process, a long-term field study should be conducted to assess the durability and uncertainty of MPDs under real-world environmental conditions.

Author Contributions: Conceptualization: D.-H.B. and T.-V.D.; data acquisition: B.-G.P. and S.-W.L.; data analysis: D.-H.B. and S.-W.L.; visualization: B.-G.P. and D.-H.B.; writing—original draft preparation: D.-H.B. and B.-G.P.; writing—review and editing: J.-C.K. and T.-V.D. All authors have read and agreed to the published version of the manuscript.

Funding: This research received no external funding.

Institutional Review Board Statement: Not applicable.

Informed Consent Statement: Not applicable.

Data Availability Statement: Data are contained within the article. More detailed data are available from the corresponding authors upon reasonable request.

Acknowledgments: This work was supported by the National Research Foundation of Korea (NRF) grant funded by the Korean government (MSIT) (No. 2023R1A2C2002956). This work was supported by the Technology Innovation Program (RS-2024-00431713, Development of equipment for measuring the global warming potential (GWP) and greenhouse gas emissions in display process) funded By the Ministry of Trade Industry & Energy (MOTIE, Korea).

Conflicts of Interest: The authors declare no conflicts of interest.

References

1. US EPA Basic Information About Air Emissions Monitoring. Available online: https://www.epa.gov/air-emissions-monitoring-knowledge-base/basic-information-about-air-emissions-monitoring (accessed on 8 April 2025).
2. WHO. *Monitoring Air Pollution Levels Is Key to Adopting and Implementing WHO's Global Air Quality Guidelines*; WHO: Geneva, Switzerland, 2023.
3. Eom, Y.-S.; Hong, J.-H.; Lee, S.-J.; Lee, E.-J.; Cha, J.-S.; Lee, D.-G.; Bang, S.-A. Emission Factors of Air Toxics from Semiconductor Manufacturing in Korea. *J. Air Waste Manag. Assoc.* **2006**, *56*, 1518–1524. [CrossRef] [PubMed]
4. Hess, J.-S.; Semenova, A. Semiconductor Emission Explorer: Tracking Greenhouse Gas Emissions from Chip Production (2015-2023), Interface. 2025. Available online: https://www.interface-eu.org/publications/semiconductor-emission-explorer (accessed on 8 April 2025).
5. Change, C. Intergovernmental Panel on Climate Change (IPCC). In *Climate Change 2021-The Physical Science Basis*; Cambridge University Press: Cambridge, UK, 2023; ISBN 9781009157896.
6. Srivastava, D.; Vu, T.V.; Tong, S.; Shi, Z.; Harrison, R.M. Formation of Secondary Organic Aerosols from Anthropogenic Precursors in Laboratory Studies. *NPJ Clim. Atmos. Sci.* **2022**, *5*, 22. [CrossRef]
7. Ma, R.; Li, K.; Guo, Y.; Zhang, B.; Zhao, X.; Linder, S.; Guan, C.; Chen, G.; Gan, Y.; Meng, J. Mitigation Potential of Global Ammonia Emissions and Related Health Impacts in the Trade Network. *Nat. Commun.* **2021**, *12*, 6308. [CrossRef]

8. Chen, Y.; Yao, B.; An, M.; Ding, A.; Liu, S.; Li, X.; Li, Y.; O'Doherty, S.; Krummel, P.B.; Yang, H.; et al. Emissions of Perfluorinated Greenhouse Gases in Southeastern China Derived From High-Frequency In Situ Observations. *Geophys. Res. Lett.* **2025**, *52*, e2024GL111393. [CrossRef]
9. Sadovnikov, S.A.; Yakovlev, S.V.; Kravtsova, N.S.; Romanovskii, O.A.; Tuzhilkin, D.A. Dual-Channel Infrared OPO Lidar Optical System for Remote Sensing of Greenhouse Gases in the Atmosphere: Design and Characteristics. *Sens. Int.* **2025**, *6*, 100307. [CrossRef]
10. Wawrzyniak, J. Quantitative Determination of Volatile Compounds in a Mixture Using a Single Thermally Modulated Metal Oxide Semiconductor Gas Sensor and Convolutional Neural Networks. *Microchem. J.* **2025**, *211*, 113083. [CrossRef]
11. Nguyen, M.T.N.; Lee, J.S. Development of a Chemical Sensor Device for Monitoring Hazardous Gases Generated in the Semiconductor Manufacturing Process. *Chemosensors* **2024**, *12*, 233. [CrossRef]
12. Lee, B.-J.; Yun, S.-Y.; Jeong, I.-K.; Hwang, Y.; Park, J.-H.; Kim, J. Improving the Measurement of Characteristic Parameters for the Determination of GHG Emissions in the Semiconductor and Display Industries in Korea. *Appl. Sci.* **2023**, *13*, 8834. [CrossRef]
13. Dinh, T.-V.; Kim, J.-C. Moisture Removal Techniques for a Continuous Emission Monitoring System: A Review. *Atmosphere* **2021**, *12*, 61. [CrossRef]
14. Kim, D.-J.; Dinh, T.-V.; Lee, J.-Y.; Son, D.-J.; Kim, J.-C. Effect of Nafion Dryer and Cooler on Ambient Air Pollutant (O_3, SO_2, CO) Measurement. *Asian J. Atmos. Environ.* **2020**, *14*, 28–34. [CrossRef]
15. Dinh, T.-V.; Choi, I.-Y.; Son, Y.-S.; Kim, J.-C. A Review on Non-Dispersive Infrared Gas Sensors: Improvement of Sensor Detection Limit and Interference Correction. *Sens. Actuators B Chem.* **2016**, *231*, 529–538. [CrossRef]
16. Dinh, T.V.; Ahn, J.W.; Choi, I.Y.; Song, K.Y.; Chung, C.H.; Kim, J.C. Limitations of Gas Filter Correlation: A Case Study on Carbon Monoxide Non-Dispersive Infrared Analyzer. *Sens. Actuators B Chem.* **2017**, *243*, 684–689. [CrossRef]
17. Kim, D.-J.; Dinh, T.-V.; Lee, J.-Y.; Choi, I.-Y.; Son, D.-J.; Kim, I.-Y.; Sunwoo, Y.; Kim, J.-C. Effects of Water Removal Devices on Ambient Inorganic Air Pollutant Measurements. *Int. J. Environ. Res. Public Health* **2019**, *16*, 3446. [CrossRef] [PubMed]
18. Gil, H.-N.; Dinh, T.-V.; Lee, J.-H.; Park, B.-G.; Choi, I.-Y.; Lee, S.-W.; Kim, I.-Y.; Kim, J.-C. Effects of Humidity Pretreatment Devices on the Loss of HCl Gas Emitted from Industrial Stacks. *Atmosphere* **2021**, *13*, 33. [CrossRef]
19. Lee, J.-Y.; Dinh, T.-V.; Kim, D.-J.; Choi, I.-Y.; Ahn, J.-W.; Park, S.-Y.; Jung, Y.-J.; Kim, J.-C. Effect of Conventional Water Pretreatment Devices on Polar Compound Analysis. *Asian J. Atmos. Environ.* **2019**, *13*, 249–258. [CrossRef]
20. Dinh, T.-V.; Kim, D.-J.; Lee, J.-Y.; Park, B.-G.; Choi, I.-Y.; Kim, I.-Y.; Kim, J.-C. Development of a Humidity Pretreatment Method for the Measurement of Ozone in Ambient Air. *J. Hazard. Mater.* **2022**, *426*, 128108. [CrossRef]
21. Lee, J.-Y.; Dinh, T.-V.; Kim, D.-J.; Choi, I.-Y.; Ahn, J.-W.; Park, S.-Y.; Jung, Y.-J.; Kim, J.-C. Comparison of Water Pretreatment Devices for the Measurement of Polar Odorous Compounds. *Appl. Sci.* **2019**, *9*, 4045. [CrossRef]
22. Lee, S.-W.; Dinh, T.-V.; Park, S.-Y.; Choi, I.-Y.; Kim, I.-Y.; Park, B.-G.; Baek, D.-H.; Park, J.-H.; Seo, Y.-B.; Kim, J.-C. Development of a Moisture Pretreatment Device for the Accurate Quantitation of Water-Soluble Volatile Organic Compounds in Air. *Chemosensors* **2023**, *11*, 188. [CrossRef]
23. Lee, E.-H.; Kim, T.-W.; Byun, S.; Seo, D.-W.; Hwang, H.-J.; Baek, J.; Kim, H.; Ryi, S.-K. A Study on γ-Al_2O_3 Catalyst for N_2O Decomposition. *Clean Technol.* **2023**, *29*, 126–134.
24. Jahnke, J.A. *Continuous Emission Monitoring*, 2nd ed.; John Wiley & Sons, Inc.: Toronto, ON, Canada, 2000; ISBN 0-471-29227-3.
25. Wilson, K.L. *Water Vapor Interference in the UV Absorption Measurement of Atmospheric Ozone*; University of Colorado: Boulder, CO, USA, 2005.
26. Son, Y.-S.; Lee, G.; Kim, J.-C.; Han, J.-S. Development of a Pretreatment System for the Analysis of Atmospheric Reduced Sulfur Compounds. *Anal. Chem.* **2013**, *85*, 10134–10141. [CrossRef]
27. Haberhauer-Troyer, C.; Rosenberg, E.; Grasserbauer, M. Investigation of Membrane Dryers and Evaluation of a New Ozone Scrubbing Material for the Sampling of Organosulphur Compounds in Air. *J. Chromatogr. A* **1999**, *852*, 589–595. [CrossRef] [PubMed]
28. Siemens ULTRAMAT 23—Advanced Analytics Made Into A Commodity. Available online: https://www.siemens.com/global/en/products/automation/process-analytics/extraktive-continuous-process-gas-analytics/ultramat-23.html (accessed on 4 April 2025).
29. envea E-Series Nitrogen Oxides Analyzer NO, NOX & NO2. Available online: https://envea.global/product/ac32e-2/ (accessed on 4 April 2025).
30. Thermo Fisher Scientific Solutions LLC NDIR Model 60 Multi-Gas Analyzer. Available online: https://www.thermofisher.com/order/catalog/product/10142556?SID=srch-srp-10142556 (accessed on 4 April 2025).
31. HORIBA Group Nitrogen Oxides Monitor. Available online: https://www.horiba.com/int/process-and-environmental/products/detail/action/show/Product/apna-380-nitrogen-oxides-monitor-6229/ (accessed on 4 April 2025).
32. Fire Testing Technology Limited FTIR. *An Advanced FTIR for Toxic Gas Analysis*; Fire Testing Technology: Sussex, UK, 2020.

33. International SEMATECH Manufacturing Initiative. *Comparison of Fourier Transform Infrared (FTIR) and Quadrupole Mass Spectroscopy (QMS) Methods for Determining POU Abatement System Effluent Flow*; International SEMATECH Manufacturing Initiative Technology Transfer: Austin, TX, USA, 2011.
34. Japan Electronics and Information Technology Industries Association. *JEITA Guideline for F-GHG Characterization and Management*; JEITA: Tokyo, Japan, 2011.
35. NIST Chemistry WebBook Ethane, Hexafluoro-. Available online: https://webbook.nist.gov/cgi/cbook.cgi?Formula=C2F6&NoIon=on&Units=SI (accessed on 5 April 2025).
36. NIST Chemistry WebBook Fluoroform. Available online: https://webbook.nist.gov/cgi/cbook.cgi?ID=C75467&Units=SI (accessed on 5 April 2025).
37. NIST Chemistry WebBook Nitrogen Trifluoride. Available online: https://webbook.nist.gov/cgi/cbook.cgi?Name=NF3&Units=SI (accessed on 5 April 2025).
38. NIST Chemistry WebBook Nitrous Oxide. Available online: https://webbook.nist.gov/cgi/cbook.cgi?ID=C10024972&Mask=10 (accessed on 5 April 2025).
39. NIST Chemistry WebBook Tetrafluoromethane. Available online: https://webbook.nist.gov/cgi/cbook.cgi?Formula=CF4&NoIon=on&Units=SI (accessed on 5 April 2025).
40. WHO. *Environmental Health Criteria 50 Trichloroethylene*; WHO: Geneva, Switzerland, 1985.
41. Rapson, T.D.; Dacres, H. Analytical Techniques for Measuring Nitrous Oxide. *TrAC Trends Anal. Chem.* **2014**, *54*, 65–74. [CrossRef]
42. Bi, Z.; Shi, Y.; Wang, Z.; Han, X.; Wang, M. Effect of Humidity on Atmospheric VOCs Measurement. *IOP Conf. Ser. Earth Environ. Sci.* **2021**, *621*, 012139. [CrossRef]
43. Hartonen, K.; Helin, A.; Parshintsev, J.; Riekkola, M.-L. Problems Caused by Moisture in Gas Chromatographic Analysis of Headspace SPME Samples of Short-Chain Amines. *Chromatographia* **2019**, *82*, 307–316. [CrossRef]
44. Zhang, X.; He, A.; Guo, R.; Zhao, Y.; Yang, L.; Morita, S.; Xu, Y.; Noda, I.; Ozaki, Y. A New Approach to Removing Interference of Moisture from FTIR Spectrum. *Spectrochim. Acta Part A Mol. Biomol. Spectrosc.* **2022**, *265*, 120373. [CrossRef]
45. Park, B.-G.; Dinh, T.-V.; Lee, S.-W.; Choi, I.-Y.; Cho, B.-C.; Baek, D.-H.; Kim, J.-C.; Kim, J.-C. Investigation of Long-Term Performance of a Proposed Cost-Effective HCl Non-Dispersive Infrared Analyzer at Real Stationary Sources. *Chemosensors* **2024**, *12*, 262. [CrossRef]
46. Dinh, T.-V.; Park, B.-G.; Lee, S.-W.; Choi, I.-Y.; Baek, D.-H.; Kim, J.-C. Long-Term Evaluation of Mid-Cost Optical Particle Counters for PM2.5 Monitoring in an Underground Subway Station: Insights from a 15-Month Study. *Chemosensors* **2025**, *13*, 25. [CrossRef]
47. Kang, Y.; Aye, L.; Ngo, T.D.; Zhou, J. Performance Evaluation of Low-Cost Air Quality Sensors: A Review. *Sci. Total Environ.* **2022**, *818*, 151769. [CrossRef]
48. Giordano, M.R.; Malings, C.; Pandis, S.N.; Presto, A.A.; McNeill, V.F.; Westervelt, D.M.; Beekmann, M.; Subramanian, R. From Low-Cost Sensors to High-Quality Data: A Summary of Challenges and Best Practices for Effectively Calibrating Low-Cost Particulate Matter Mass Sensors. *J. Aerosol Sci.* **2021**, *158*, 105833. [CrossRef]
49. Nguyen, D.H.; Ahn, H.S. A Comprehensive Review on Micro/Nanoscale Surface Modification Techniques for Heat Transfer Enhancement in Heat Exchanger. *Int. J. Heat Mass Transf.* **2021**, *178*, 121601. [CrossRef]
50. Zhang, X.; Tian, W.; Li, J.; Han, Z.; Wu, X. Effects of Coolant Temperature on Particulate Deposition and Cooling Efficiency of EGR Coolers. *J. Mech. Sci. Technol.* **2021**, *35*, 3231–3237. [CrossRef]
51. Suarez-Romero, J.G.; Rodriguez-Valdelamar, J.L. *Fourier Theory in Temperature Measurements*; Kahan, M.A., Ed.; Optical Engineering + Applications: San Diego, CA, USA, 2009; p. 74270C.
52. Rohlfs, W.; Lienhard V, J.H. Entrance Length Effects on Graetz Number Scaling in Laminar Duct Flows with Periodic Obstructions: Transport Number Correlations for Spacer-Filled Membrane Channel Flows. *Int. J. Heat Mass Transf.* **2016**, *97*, 842–852. [CrossRef]
53. Romero-Trigueros, C.; Doval Miñarro, M.; González Ferradás, E. Influence of Environmental Humidity on Measurements of Benzene in Ambient Air by Transportable GC-PID. *Atmos. Meas. Tech.* **2017**, *10*, 4013–4022. [CrossRef]
54. US Agency for Toxic Substances and Disease Registry. *Toxicological Profile for Trichloroethylene*; ATSDR: Atlanta, GA, USA, 2020.
55. US National Library of Medicine Nitrous Oxide. Available online: https://pubchem.ncbi.nlm.nih.gov/compound/Nitrous-Oxide (accessed on 14 February 2025).
56. Paidar, M.; Mališ, J.; Bouzek, K.; Žitka, J. Behavior of Nafion Membrane at Elevated Temperature and Pressure. *Desalination Water Treat.* **2010**, *14*, 106–111. [CrossRef]

Disclaimer/Publisher's Note: The statements, opinions and data contained in all publications are solely those of the individual author(s) and contributor(s) and not of MDPI and/or the editor(s). MDPI and/or the editor(s) disclaim responsibility for any injury to people or property resulting from any ideas, methods, instructions or products referred to in the content.